INTERNATIONAL JOURNAL OF AUTOMOTIVE AND MECHANICAL ENGINEERING
ISSN: 2229-8649 e-ISSN: 2180-1606
VOL. 21, ISSUE 3, 2024, 11486 – 11501
DOI: https://doi.org/10.15282/ijame.21.3.2024.3.0886

RESEARCH ARTICLE

A Simplified Failure Assessment to Identify Crack Growth Behavior in the Gas Pipeline by Post-Hydrostatic Pressure

F. M. Assidiq[1]*, Juswan[1], D. Paroka[1], T. Rachman[1], R. Japri[1] and S. Wahyudi[2]

[1]Deparment of Ocean Engineering, Universitas Hasanuddin, 92119 Gowa, Indonesia
[2]PT. Kaliraya Sari, 75264 Kutai Kartanegara, Indonesia

ABSTRACT - Hydrostatic pressure tests on pipelines have been found to be an inadequate means of critical integrity management due to the frequency of false negatives, which result from the inability of these tests to detect crack growth. It can be argued that focusing on pipe leakage does not guarantee future operability. A study presents a failure assessment methodology based on the failure assessment diagram (FAD), which aims to predict crack growth during hydrotesting. The calibrated pipe spool is validated by the application of data from hydrostatic tests and analytical techniques to ascertain the potential growth in circumferential surface cracks. A variety of factors, including pressure, material grades, flaw dimensions, and elliptical flaw angles, were examined in an effort to assess cracks. The results demonstrate that there is no pipeline leakage and minimal trapped air. Despite its location within the plastic zone, with a normalized pressure index of ≤1, the pipeline is deemed to be within acceptable limits according to the criteria established by the FAD. The assessment point was found to be predominantly influenced by the toughness ratio of the material grade. The crack propagated in the opposite direction with a maximum length *a/c*= 0.125 and a crack depth *a/t*= 0.2, which limited the toughness ratio. The load ratio indicates uniformity in elliptical angle flaw results. In this simplified failure assessment, the parameter describing the flaw size, which exhibits a strong correlation with the toughness ratio, plays a pivotal role. Further research and recommendations are also proposed.

ARTICLE HISTORY
Received : 18th Sept. 2023
Revised : 14th May 2024
Accepted : 20th June 2024
Published : 20th Sept. 2024

KEYWORDS
Crack growth behavior
Failure assessment
Gas pipeline
Post-hydrostatic pressure
Trapped air

1. INTRODUCTION

The basic approach for establishing the persistent mechanical serviceability of pipelines containing water and/or gas under maximum allowable operating pressure (MAOP) is the hydrostatic pressure test [1-3]. All sectors perform these tests to evaluate the integrity of recently constructed pipelines prior to their operation [4-6]. Furthermore, in terms of costs and flow rate, it is a viable alternative to common in-line inspection [7]. Hydrotesting, on the other hand, is not suggested in high-integrity criticality circumstances because it excludes the defect dimensions fundamental for future integrity management [8-9]. This indicates that hydrotesting fails to observe fractures related to fatigue growth at high material toughness. Other drawbacks are discussed in [10].

Cracking is one of the aberrant causes that might occur during the installation and operation stages [11-12]. Cracks are the result of repetitive hydrotesting over a lengthy period of time. During the service life, cracks are induced to expand cumulatively. Its contribution frequently manifests in plastic collapse scenarios, which in all cases threaten the failure of pipes composed of moderately ductile materials [13]. Moreover, it will exhibit significant deformation [14-17]. Other factors belong to crack depth and crack length, which could have a major and unpredictable impact on the pipeline's integrity [18]. Pipelines with shallow crack depths typically fail owing to plastic collapse, whereas those with large crack depths fracture. Meanwhile, increased fracture length growth permits the pipeline to endure further pressure. This depends on the plasticity, which interrupts the growth of the crack tip [14], [19], [20].

Material properties must also be carefully considered. The degradation produced by prior operations should be reflected in the pipeline material, which is an indicator of integrity assessment. Hence, material attributes should be employed to calculate the optimal crack opening area estimation [21]. The inadequacy of hydrotesting to detect faults may generate uncertainty regarding the service life of pipelines. Excessive hydrotesting, for example, has the potential to trigger pipe rupture and lateral bending in the pipeline's free span [9], [11]. This is greatly dependent on the pressure testing cycle and the holding time itself. Consequentially, the pipeline will encounter pressure reversal and, ultimately, failure. The exceptionally high-stress intensity of hydrotesting, on the other hand, may reduce crack propagation due to crack blunting in front of the crack tip [22].

The preceding review of literature illustrates that, despite numerous hydrotesting investigations, the primary focus has been on pipe leakage and crack propagation in specific, often idealized, scenarios. This narrow approach hinders a comprehensive assessment of the actual effects of hydrotesting on the integrity of pipelines. It is widely recognized that hydrotesting has the potential to introduce residual stresses, initiate microcracks, and even blunt pre-existing cracks, all of which could significantly impact the long-term performance of a pipeline. Therefore, in addition to addressing

*CORRESPONDING AUTHOR | F. M. Assidiq | ✉ assidiqfm@unhas.ac.id

immediate concerns such as leakage and short-term crack growth during hydrotesting, the incorporation of a failure assessment diagram (FAD) is essential for evaluating the long-term implications of crack propagation over the pipeline's operational lifespan [23-24]. The interplay of fracture and plastic collapse mechanisms is demonstrated by FAD. It evaluates three main elements: point of assessment, applied load ratio, and toughness ratio. These factors are determined by considering defect size, material properties, and pressure. Other beneficial implications for FAD in decision-making can be identified in [25-27].

Given the potential influence of FAD, this study investigates its role in accurately assessing the integrity of a system during hydrotesting. It will, in particular, present an alternative viewpoint on completing hydrotesting investigations in a simplified manner, emphasizing the methodology used in this study. In Section 2 of the study, the experimental approach to the spool pipeline is discussed, along with several other attributes to be examined based on FAD. Section 3 provides a detailed examination of the hydrotesting proof, normalized pressure, material properties, flaw size, and flaw elliptical angle. Finally, Section 4 presents the conclusion and proposed recommendation.

2. METHOD

This study was conducted on API 5L X65 hard-carbon commercial steel pipe. Comparatively low cost, good weldability, and superior mechanical properties are some of the advantages of carbon steel [28-30]. This spool pipe is commonly found in oil and gas pipelines [31]. Its steel mechanical properties are shown in Table 1 [32-36]. To transmit the gas liquid to the next station, the spool pipe is 0.2 km long, 84 mm in outer diameter (R_o), and 9.5 mm thick (t). The essential components required at the site for hydrotesting are presented in Figure 1 and Table 2. Furthermore, instrument ambiguity is always an issue during testing, particularly during hydrotesting [37]. The calibration of all instruments utilized has been completed. This is consistent with the accuracy of all instruments, which are precise and competent.

Table 1. Mechanical properties of proposed spool pipe

Material Grade	Yield strength σ_y (MPa)	Ultimate strength σ_{ul} (MPa)	Material toughness K_{IC} (MPa√m)
X56	386	490	188
X60	414	517	250
X65	465	558	280
X70	483	565	330

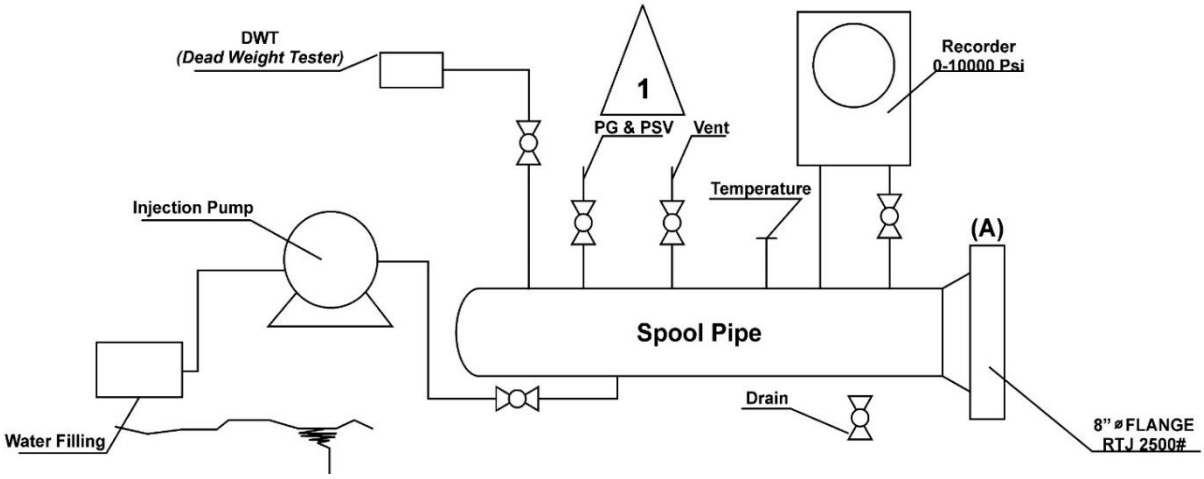

Figure 1. Hydrotesting scheme

Table 2. Equipment list for hydrotesting

Instrument	Remark
Flowmeter	Fill the spool pipe with water and record its volume
Pressurizing flowmeter	Determine and note the volume of water injected into the spool pipe
Deadweight tester (DWT)	Given an accuracy of ±0.05%, analyze and document the pressure
Pressure gauge	Given ±0.1% accuracy, record and monitor pressure
Chart recorder	Given ±0.5% precision, record and monitor pressure
Ambient air temperature recorder	Given ±1% precision, accurately gauge and record the ambient temperature

Moreover, the success of the hydrotesting depends mainly on the amount of water and air trapped. Eq. (1) can be used to calculate the volume of water needed to fill pipe V, assuming it has a perfectly cylindrical shape. However, in reality, the required water volume may be slightly increased due to factors like irregularities in the geometry and the existence of valves and fittings [38].

$$V = 0.0204{R_i}^2 L \tag{1}$$

where the variable R_i represents the pipe inner radius, while L denotes the pipe length. When water inside a pipe experiences high pressure, it undergoes slight compression in volume. Furthermore, variations in water and pipe temperature can also have an impact on its volume. To accommodate these variables, the equation for water volume under pipe pressure V_{tp} incorporates a correction factor that considers water's compressibility F_{wp}, changes in pipe volume F_{pp}, and alterations in water and pipe volume caused by temperature changes F_{pwt} as demonstrated in Eq. (2).

$$V_{tp} = V F_{wp} F_{pp} F_{pwt} \tag{2}$$

with

$$F_{wp} = \frac{14.73P}{1.0 - (4.5 \times 10^{-5})} \tag{3}$$

$$F_{pp} = 1.0 + \left[\left(\frac{2R_o}{t}\right)\left(\frac{0.91P}{30 \times 10^6}\right)\right] \tag{4}$$

$$F_{pwt} = \frac{F_{pt}}{F_{wt}} \tag{5}$$

$$F_{pt} = 1.0 + [(T - 60)18.2 \times 10^{-6}] \tag{6}$$

where the test pressure is denoted as P, the pipe temperature as T, the factor to correct for changes in pipe volume due to thermal expansion of the pipe from a base temperature of 16°C as F_{pt}, and the factor to correct for the specific thermal change in water volume from 16°C to test water temperature as F_{wt}, as described in [38].

The results of the tests may be affected by air that has accumulated within the pipe during hydrotesting. The calculation and control of the amount of this air is therefore essential. In this process, Boyle's Law, as explained in Eq. (7), becomes a useful tool for determining the pressures and volumes of gas.

$$P_1 V_1 = P_2 V_2 \tag{7}$$

where P_1 is the initial gas pressure, P_2 is the final gas pressure, V_1 is the initial gas volume, and V_2 is the final gas volume.

Acceptance criteria have been set for confined air in order to guarantee the reliability of this test [39]. In order to reduce the influence of air on test results and ensure that assessment accuracy is achieved, this criterion stipulates that no more than 0.2% of total water volume should be affected by trapped air percentage V_{at}, as described in Eq. (9).

$$V_1 = V + V_{tp} \tag{8}$$

$$\begin{gathered} V_{at} = V_{pc}(V_1 + V_2) \\ V_{at} \leq 0.2\% \end{gathered} \tag{9}$$

where V_{pc} is the volume of trapped air, which will be given in Figure 9.

Following hydrotesting, a failure assessment diagram (FAD) methodology is implemented to evaluate the crack size when the failure occurs [24]. Figure 2(a) depicts the circumferential crack surface associated with spool pipe failure. This type of crack is among the most significant defects in tubular structures [40-41]. Although cracks of diverse orientations may arise in the pipe wall, this analysis will concentrate on semi-elliptical internal cracks. These cracks are particularly susceptible to hoop stress as a consequence of hydrotesting P_h on the inner surface of the pipe wall.

The stress field and stress intensity factor along the semi-elliptical crack front in the spool pipe are determined by various influential factors. These factors include the crack length a/c, crack depth a/t, crack elliptical angle φ, and thickness-to-inner radius ratio t/R_i. In this study, the semi-elliptical crack model, as depicted in Figure 2(b), is utilized to investigate the impact of these factors on the stress distribution and intensity factor. By considering these parameters, a comprehensive understanding of the behavior of the spool pipe under hoop stress can be achieved.

The propagation of crack mode I in a pressurized spool pipe is characterized by the presence of a semi-elliptical crack. This type of crack occurs when the crack surfaces are pulled apart perpendicular to the crack plane due to circumferential tensile stress. The stress distribution near the crack tip, denoted as $\sigma_{(z)}$, exhibits a distinct pattern, with the side of the crack facing the applied load experiencing higher stress levels. This phenomenon is illustrated in Figure 2(c).

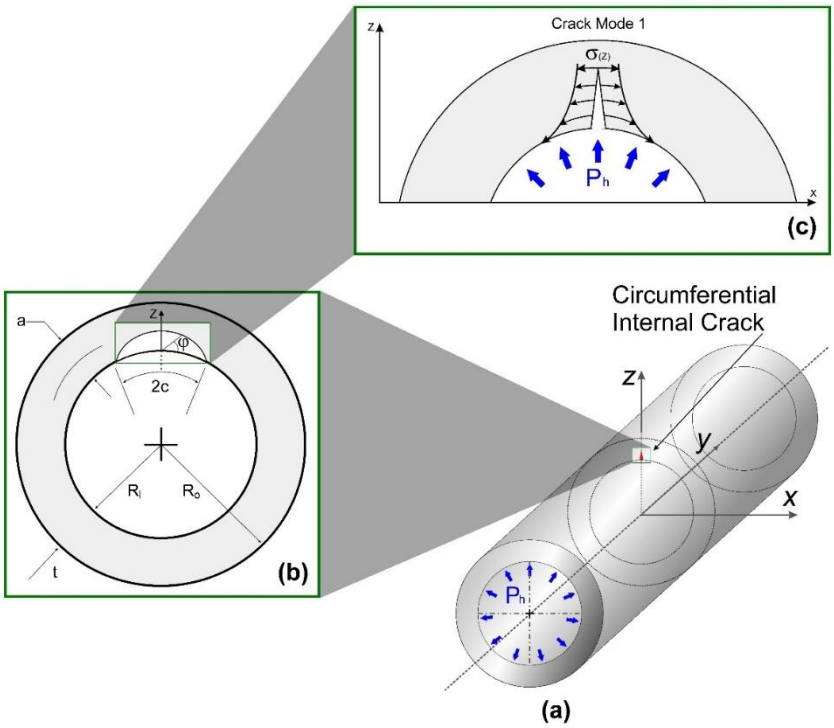

Figure 2. Configuration of a pressurized spool pipe; (a) circumferential internal surface crack location, (b) semi-elliptical crack parameters notation, and (c) stress distribution on crack opening mode I.

As shown in Figure 3, the determination of the stress analysis acceptability involves the combination of different factors, including stress intensity factor K_I, fracture toughness K_{IC}, material yield strength σ_y, and reference stress solution σ_{ref}, as provided in Table 1, Eq. (11), and Eq. (21). These factors utilized to calculate the load ratio L_r, and toughness ratio K_r are indicated in Eq. (10) and Eq. (20), which represent the coordinates of an assessment point on a two-dimensional FAD. The assessment point is then employed to evaluate the acceptability of the stress analysis outcomes.

Furthermore, the FAD diagram contains an envelope line as a failure factor between acceptable and unacceptably situated regions. The component shall be acceptable for continued operation if the assessment point is at or beneath the FAD envelope and vice versa. Moreover, the FAD diagram encompasses three crucial distribution zones. The elastic-plastic zone (0º-30º), the elastic-plastic zone (30º-60º), and the elastic zone (60º-90º) are identified according to their angles, which are measured from the horizontal line [42]. The elastic zone anticipates the majority of fracture control and corresponds with brittle fracture. The following zone implies an elastic-plastic fracture failure mode, while the final zone represents collapse-controlled forecasting with broad results resulting in massive deformations. All of these schematic zones provide a choice on whether the spool pipe can be used indefinitely.

$$L_r = \frac{\sigma_{ref}}{\sigma_y} \tag{10}$$

$$\sigma_{ref} = \frac{gP_b + [(gP_b)^2 + 9(M_s P_m (1.0-\alpha)^2)^2]^{0.5}}{3(1.0-\alpha)^2} \tag{11}$$

with

$$g = 1.0 - 20\left(\frac{a}{2c}\right)^{0.75}\alpha^3 \tag{12}$$

$$\alpha = \frac{\frac{a}{t}}{1.0+\frac{t}{c}} \tag{13}$$

$$P_b = \frac{p_h}{2} \tag{14}$$

$$P_m = \frac{p_h R_i}{t} \tag{15}$$

$$M_s = \frac{1.0}{1.0 - \frac{a}{t} + \frac{a}{t}\left(\frac{1.0}{M_t \lambda_a}\right)} \tag{16}$$

$$M_t = \left(\frac{1.0078 + 0.10368\lambda^2 + 3.7894(10^{-4})\lambda^4}{1.0 + 0.021979\lambda^2 + 1.5742(10^{-6})\lambda^4} \right)^{0.5} \tag{17}$$

$$\lambda_a = \frac{1.818c}{\sqrt{R_i a}} \tag{18}$$

$$\lambda = \frac{1.818c}{\sqrt{R_i t}} \tag{19}$$

The given Eq. (12-19) involves various parameters related to reference stress σ_{ref} in a cylindrical shell. These parameters include the reference stress bending parameter g, the reference stress parameter α, the through-wall primary bending stress parameter P_b, the primary membrane stress component P_m, the surface correction factor M_s, the correction factor for a through-wall crack M_t, the cylindrical shell parameter λ, and the cylindrical shell resistance parameter λ_a.

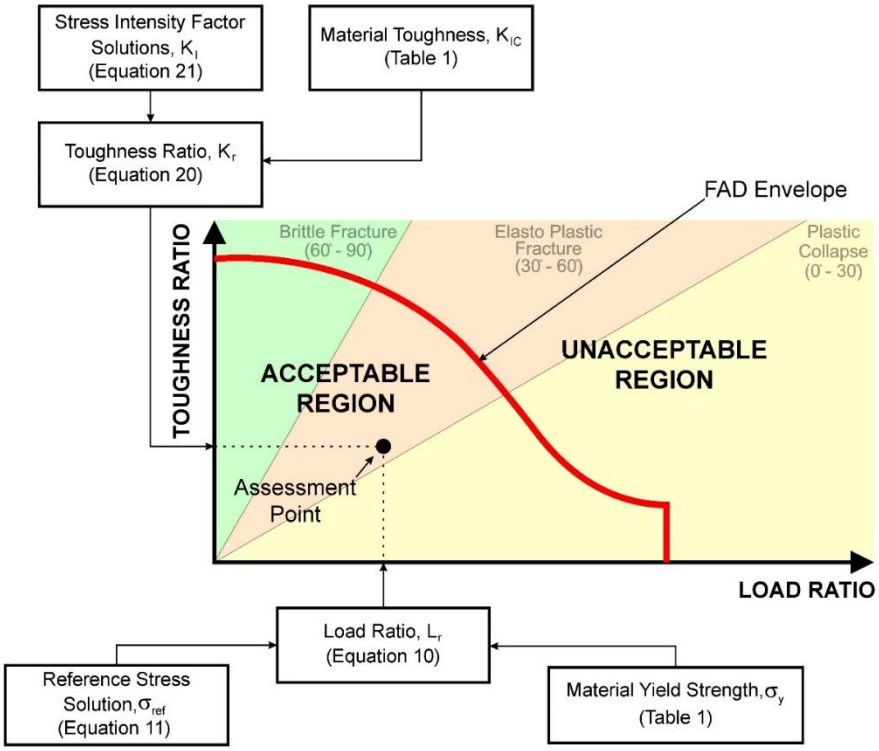

Figure 3. Overview of FAD methodology

$$K_r = \frac{K_I}{K_{IC}} \tag{20}$$

$$K_I = G_0 \left(\frac{P_h {R_o}^2}{{R_o}^2 - {R_i}^2} + \frac{F}{\pi\left({R_o}^2 - {R_i}^2\right)} \right) \sqrt{\frac{\pi a}{Q}} \tag{21}$$

with

$$G_0 = A_{0,0} + A_{1,0}\beta + A_{2,0}\beta^2 + A_{3,0}\beta^3 + A_{4,0}\beta^4 + A_{5,0}\beta^5 + A_{6,0}\beta^6 \tag{22}$$

$$\beta = \frac{\pi\left(1 - \frac{a}{t} - \frac{P_m}{\sigma_y}\right)}{2 - \frac{a}{t}} \tag{23}$$

$$F = 0.97\left[M_1 + M_2 \left(\frac{a}{t}\right)^2 + M_3 \left(\frac{a}{t}\right)^4 \right] g_s f_\varphi f_c \tag{24}$$

$$M_1 = 1.13 - 0.09\frac{a}{c} \tag{25}$$

$$M_2 = -0.54 + \frac{0.89}{0.2 + \frac{a}{c}} \tag{26}$$

$$M_3 = 0.5 - \frac{1.0}{0.65 + \frac{a}{c}} + 14\left(1.0 - \frac{a}{c}\right)^{24} \tag{27}$$

$$g_s = 1.0 + \left[0.1 + 0.35\left(\frac{a}{t}\right)^2\right](1.0 - \sin^2\varphi)^2 \tag{28}$$

$$f_\varphi = \left[\sin^2\varphi + \left(\frac{a}{c}\right)^2 \cos^2\varphi\right]^{1/4} \tag{29}$$

$$f_c = \left(\frac{{R_o}^2 - {R_i}^2}{{R_o}^2 + {R_i}^2} + 1.0 - 0.5\sqrt{\frac{a}{t}}\right)\frac{t}{R_i} \tag{30}$$

$$\begin{aligned} Q &= 1.0 + 1.464\left(\frac{a}{c}\right)^{1.65} \qquad for\ a/c \le 1.0 \\ Q &= 1.0 + 1.464\left(\frac{c}{a}\right)^{1.65} \qquad for\ a/c > 1.0 \end{aligned} \tag{31}$$

Eq. (22-31) includes multiple parameters that contribute significantly to determining the stress intensity factor of a circumferential internal surface crack. The aforementioned parameters include the influence coefficient G_0, inner diameter crack parameter A_{n0}, reference stress parameter β, shape function for stress intensity factor F, weight function M_n, shape parameter of stress intensity g_s, flaw elliptical parameter f_φ, flaw size parameter f_c, and flaw shape parameter Q.

3. RESULTS AND DISCUSSION

Hydrostatic pressure crack growth checks were performed to evaluate the integrity of the spool pipe. The semi-elliptical internal surface crack was examined in detail. In addition, the circumferential direction and crack mode I, both of which are aspects of crack propagation, were assessed [11]. In this investigation, the event of hydrostatic test pressure is studied on the basis of a Failure Assessment Diagram (FAD) according to the consideration of its analytical sensitivity parameters, namely the normalized pressure P_N, the material grades, the flaw size, and the flaw elliptical angle φ. The results obtained from the experimental tests are reported in the following sections.

3.1 Hydrotesting Verifications

This hydrotesting procedure sequence incorporates restrictions from [43-44]. A pump with a capacity of 225 m^3/min and a speed of 1450 rpm was employed. The operating fluid is fresh water mixed with the Multitreat 5549R. In order to achieve full capacity in the spool pipe, a total combined freshwater volume V of 2802 liters is essential. This specific volume is crucial to guarantee that the pipe is completely filled, leaving no vacant space within its confines.

Additionally, there are three stages of pressure application, namely when the deadweight tester is at 35%, 70%, and 100% with a holding time of 2 hours, as indicated in the load histogram in Figure 4. The pressure hits 1600 Psi at a level of 35%, while the temperature recorder reads 38ºC. The surrounding ambient temperature is indicated at 37ºC, as illustrated in Figure 5. Moreover, Figure 6 shows that the pressure was subsequently raised by 70% to a value of 3200 Psi. This increase in pressure coincided with the temperature recorder indicating a temperature of 38ºC, while the ambient temperature stood at 37ºC. The peak pressure, depicted in Figure 7, is attained at roughly 4500 Psi with a change in recorder temperature of 41ºC while maintaining the ambient temperature constant. It's worth noting that the temperature recorder and ambient temperature were 43º and 38ºC for 2 hours, respectively. This indicates that the internal temperature of the spool pipe has risen. The investigation also revealed that approximately 2759 liters of water V_{tp} were necessary to achieve the desired test pressure. Subsequently, the depressurizing phase was executed gradually from a full pressure of 100% to complete depressurization at 0%, with a noticeable time delay, as illustrated in Figure 8. The total water volume required during the test V_1 was roughly 5561 liters, based on this test. Furthermore, 88.2 liters of water V_2 were injected during the hunt for trapped air.

The goal of this verification is to identify whether the spool pipeline has a crack-based leak utilizing the previously mentioned pressure. Figure 9 shows the phenomenon of trapped air in the internal spool pipeline, often known as the *P-V* curve. It is important to point out that the trapped air volume acquired by the straight line V_{pc} produced was 39 liters. According to [36], the curve still has to be processed further. The experimental findings of this hydrotesting reveal that the proportion of trapped air in the spool pipe V_{at} is 0.006%, which passes the criteria for analytical trapped air acceptance [45]. Furthermore, once it has been determined that the spool pipe does not leak, the FAD examination can be carried out as described in the next subsection. However, the data indicates t/R_i = 0.14, when the ratios specified in [24] are only t/R_i = 0.1 and 0.2. As a result, the prudent selection of these two ratios took into consideration the spool pipe's structural integrity.

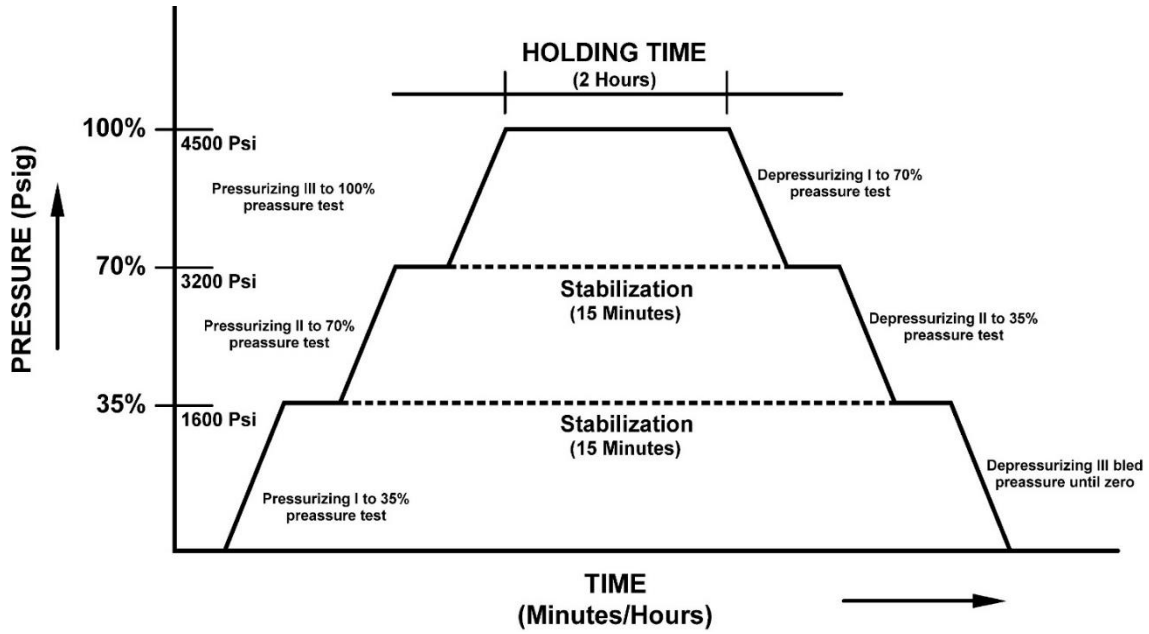

Figure 4. Load histogram of its hydrotesting

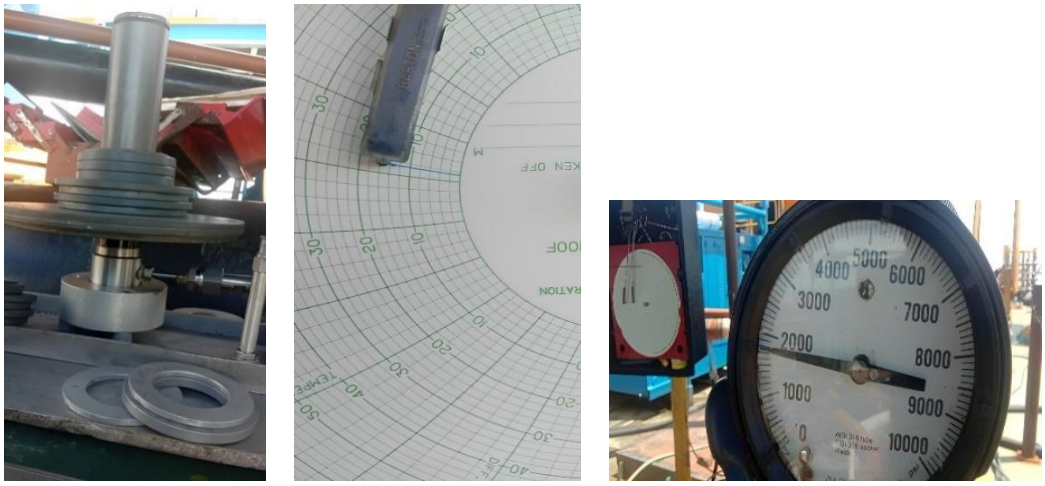

(a) (b) (c)

Figure 5. Pressurizing level at 35%. Proof of test results on (a) DWT, (b) chart recorder, and (c) pressure gauge

(a) (b) (c)

Figure 6. Pressurizing level at 70%. Proof of test results on (a) DWT, (b) chart recorder, and (c) pressure gauge

(a) (b) (c)

Figure 7. Pressurizing level at 100%. Proof of test results on (a) DWT, (b) chart recorder, and (c) pressure gauge

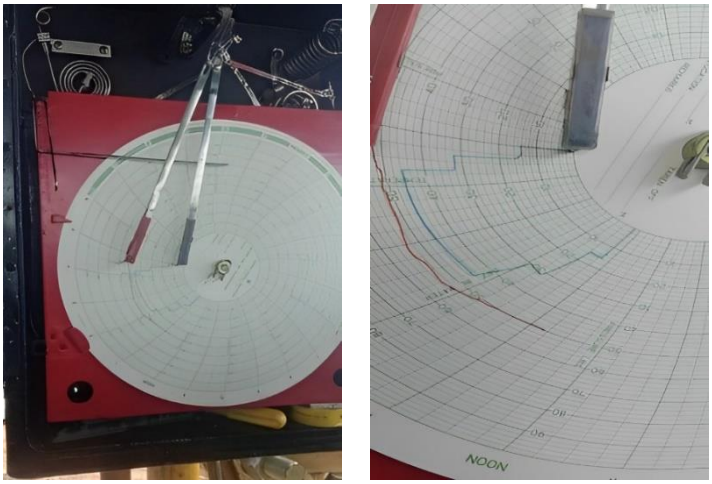

Figure 8. Depressurizing level results from 100% to 0%

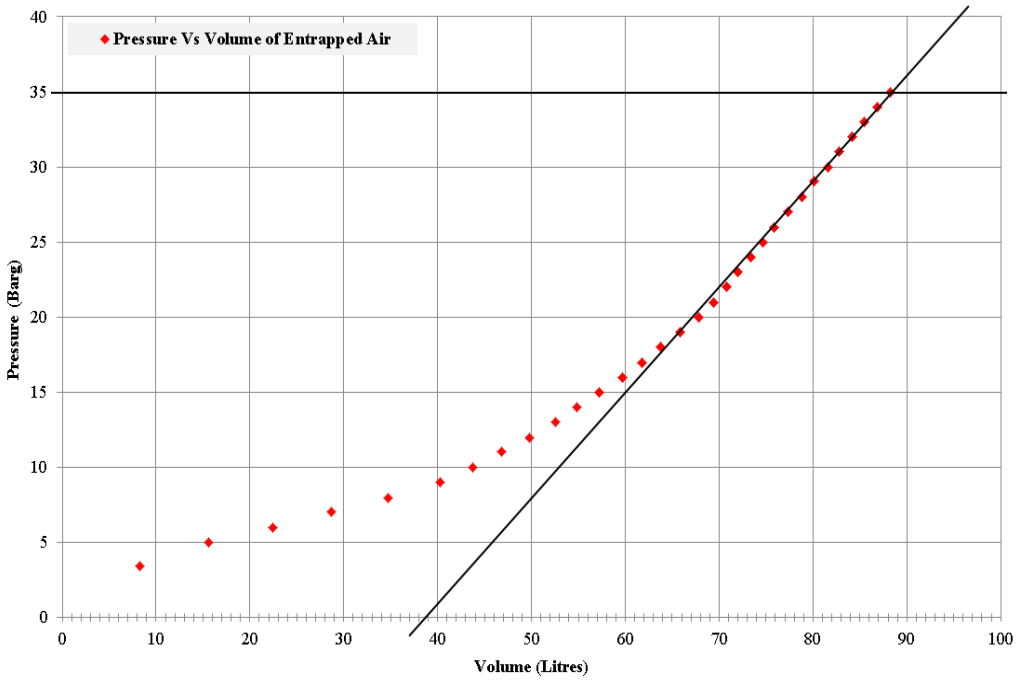

Figure 9. *P-V* curve

3.2 Normalized Pressure (P_N)

After hydrotesting verification of no leakage is obtained in the previous subsection, it is necessary to investigate the working pressure through direct testing and analytical calculations based on the relevant regulations [23], [24]. The effect of pressure on assessment points according to various flaw parameters and t/R_i ratio is listed in Figure 10. Internal and external pressures are also included in this investigation to resemble real conditions. To simplify the definition of the pressure that acts and reaches the collapse strength, normalized pressure P_N becomes a new measurement index for further regulation, which is the division of a certain incremental pressure into the existing maximum hydrotesting. Note that 0.6, 0.8, 1.0, 2.0, and 3.0 are representations of normalized pressure, respectively. It can be observed that the assessment points, condition t/R_i = 0.1 and 0.2, dominate the plastic zone based on the acceptable region. The larger normalized pressure, along with the assessment point, increases sharply in the unacceptable plastic region. This indicates that the deformation of the spool pipe that will occur will not return to the original, or, in other words, low ductility, at each normalized pressure.

The correlation between normalized pressure and load ratio L_r is interrelated, although the parameters under review have unnoticeable differences. Meanwhile, normalized pressure and toughness ratio K_r are less related to each other. This is due to the hydrotesting loads acting and the propagation of crack growth in depth. From the visible phenomenon, it can be seen that the load ratio L_r = 0 - 1 only has a significant role in the assessment point compared to the toughness ratio K_r. On the other hand, when the load L_r is greater than 1, the toughness ratio K_r has a great influence on the assessment point position.

Finally, basically, the spool pipe will experience a plastic region condition when the normalized pressure is greater than 1. It is also useful to investigate collapse strength as a supporting aspect of this failure assessment. Although some assessment points are in the elastic or elastic-plastic region, this is only a minority with special treatment in future spool inspections. Based on this information, not only the yield strength assessment but also the ultimate strength will be easily recognized [46-47]. To mitigate the collapse of the spool pipe, it is suggested that the normalized pressure should be smaller than or equal to 1 to estimate the safety of failure during hydrotesting conditions. Moreover, the assessment point can be said to be feasible to accept pressure based on experimental testing in the previous subsection. Other factors will be explained in the next subsection.

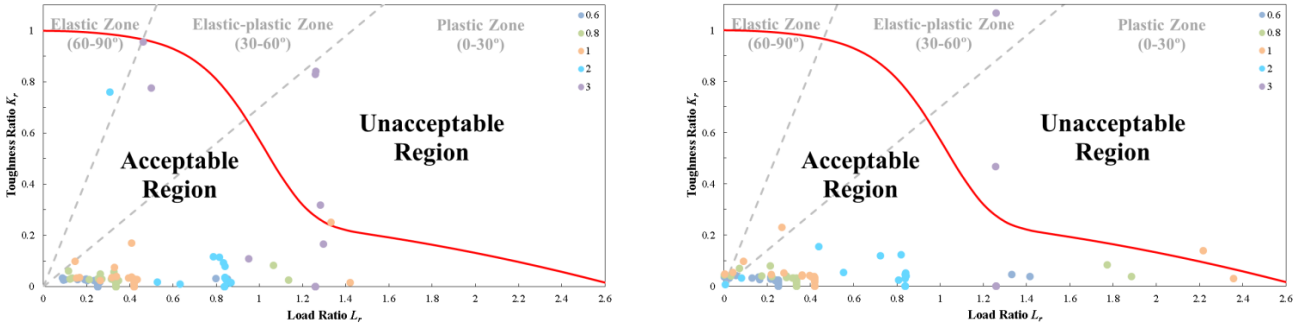

(a) t/R_i = 0.1 (b) t/R_i = 0.2

Figure 10. Assessment points for normalized pressure P_N at different t/R_i ratios

3.3 Material Grade

The effect of material grade on assessment points based on normalized pressure variation P_N and t/R_i difference is illustrated in Figure 11. This section selects and compares the X65 grade against the common grades in widely applied gas pipelines such as X56, X60, and X70 [48]. In general, the distribution of the dominant assessment point indicates that it belongs to the plastic zone. The greater the normalized pressure, the greater the chance of the assessment point falling into the plastic zone category. This is more significantly influenced by the toughness ratio K_r. If the toughness ratio K_r is greater than 1, the chance of the assessment point becoming an unacceptable region increases. On the other hand, the influence of load ratio L_r is not too great on the determination of material grade.

Another thing to note is that normalized pressure, both when t/R_i = 0.1 and 0.2, has a role in determining the assessment point. The effect will lead to a massively unacceptable plastic region. The movement of the assessment point will be equivalent to a continuous increase in toughness ratio K_r and load ratio L_r, better known as plastic collapse. The greater the normalized pressure of the internal load, the greater the chance of plastic collapse in all material grades.

Furthermore, the relationship between material grade and t/R_i ratio also affects the location of the assessment point under review. The failures of all material grades tend to increase as the t/R_i ratio increases. With this increase, there are more assessment point positions, so the condition of the spool pipe will experience an inevitable collapse. Compared to the previous explanation of the failure assessment correlation, the results of this section show a more relevant influence on the selection of spool pipe materials. This is due to the adjustment of pipe quality and economic aspects, without forgetting the consideration of gas distribution [49]. The better the material grade selected, the safer the pipe will be in

delivering gas and minimizing operating failures. Therefore, it is recommended that gas delivery performance be improved by selecting material grades above X65.

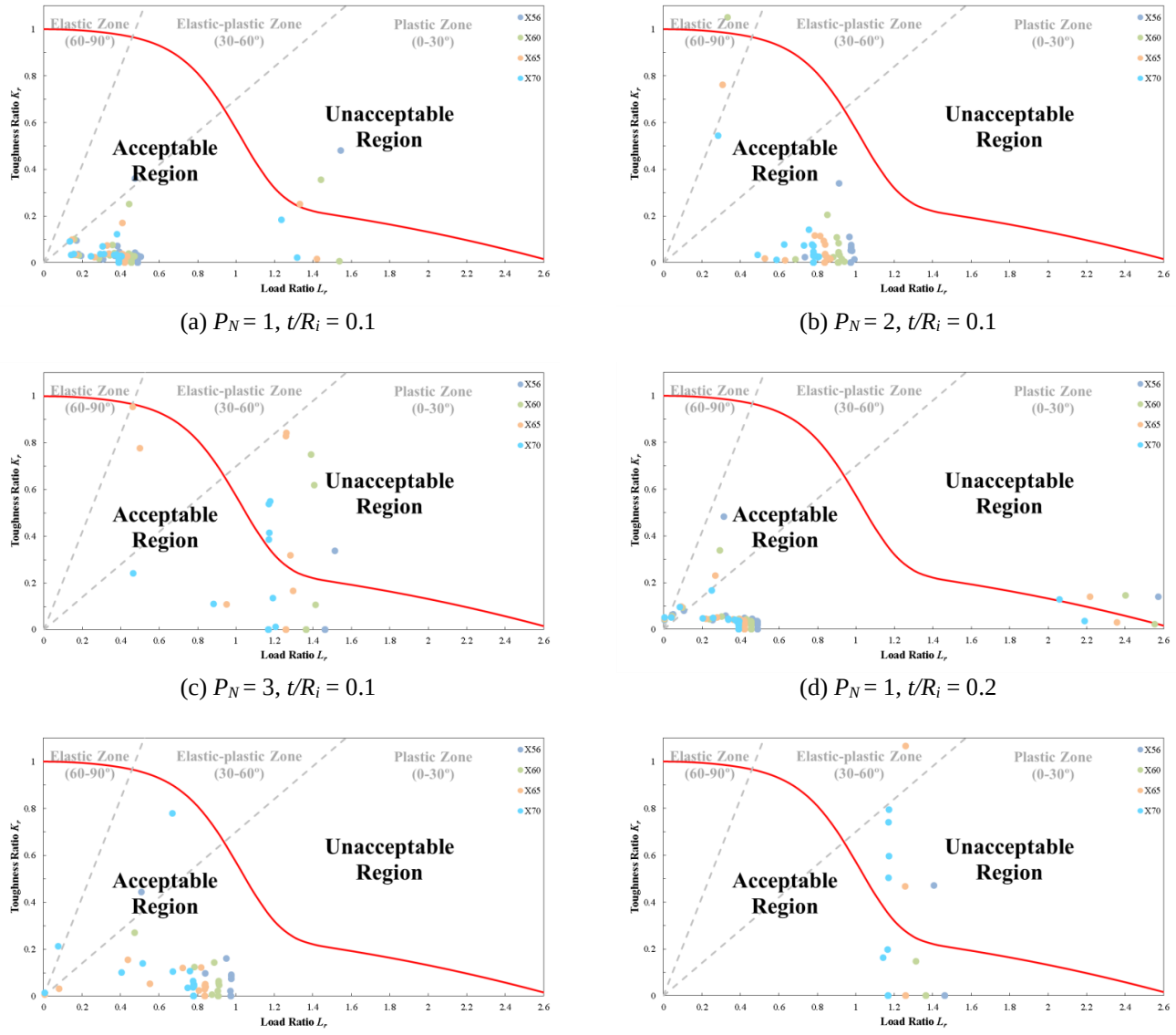

(a) $P_N = 1$, $t/R_i = 0.1$

(b) $P_N = 2$, $t/R_i = 0.1$

(c) $P_N = 3$, $t/R_i = 0.1$

(d) $P_N = 1$, $t/R_i = 0.2$

(e) $P_N = 2$, $t/R_i = 0.2$

(f) $P_N = 3$, $t/R_i = 0.2$

Figure 11. Assessment points for material grades at different P_N and t/R_i

3.4 Flaw Size

The effect of flaw size on assessment point according to the variation of normalized pressure P_N and t/R_i ratio is variously presented in Figure 12. It should be noted that the intended flaw sizes are crack length a/c of 0.03125, 0.0625, 0.125, 0.25, 0.5, 1.0, and 2.0, as well as crack depth a/t of 0, 0.2, 0.4, 0.6, and 0.8. In general, the assessment point appears to be in the acceptable plastic zone. The position of the failure point at the ratio $t/R_i = 0.1$ has a significant difference compared to $t/R_i = 0.2$. In addition, the average failure point also reaches the plastic collapse zone upon the review of various crack lengths and crack depths. These initial thoughts show that the contribution of crack length and crack depth play a significant role. Furthermore, the effect of crack depth is more significant in entering the plastic collapse zone than crack length. This is thanks to the contribution of reducing the thickness of the spool pipe, which causes crack propagation to arise more swiftly [50].

In addition, the relationship between crack length a/c and load ratio L_r is somewhat influential because of the tendency of the assessment point position to move slightly at each normalized pressure. The relationship with the toughness ratio K_r is also similar. It can therefore, be demonstrated that as the crack widens, the rate of crack propagation becomes less rapid. Transverse crack propagation is the main cause of this. In addition, the widening of crack growth is almost similar between the ratios $t/R_i = 0.1$ and 0.2. The trend is a secondary effect of crack assessment according to crack length. As a result, only the dimensional parameters of the spool pipe contribute to this crack growth.

On the other hand, the effect of the correlation between crack depth a/t and load ratio L_r is quite significant. This shows that the change in assessment point position tends to be stagnant in all normalized pressure variations. In contrast

to the correlation of the toughness ratio K_r, the position of the assessment point has shifted dramatically, increasing the prospect of accessing the unacceptable plastic collapse zone. As a result, the pipe material due to the crack process plays a greater role than the thickness itself. The deeper the crack formed, the dominant failure point was, the faster the crack propagated towards the unacceptable region. In addition, the progressive increase in the depth of crack growth only occurs at a ratio of t/R_i = 0.2, which means the thickness of the pipe is thinning. It is proven that if L_r is greater than 1, it will enter the unacceptable region. In essence, the result of crack depth shows a relevant effect in crack growth investigation accurately compared to crack depth. More thoroughly, it is expected to mitigate failure points in safety factor considerations by estimating the maximum crack length approximately a/c = 0.125 and the maximum crack depth a/t = 0.2.

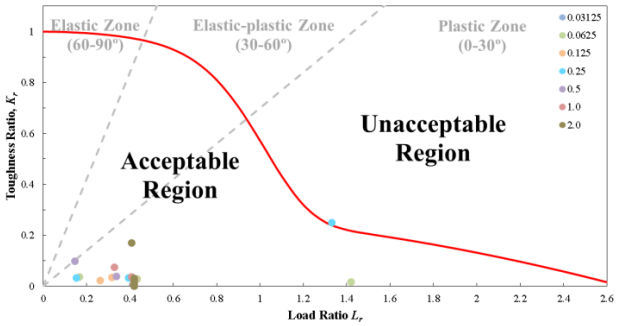

(a) P_N = 1, t/R_i = 0.1

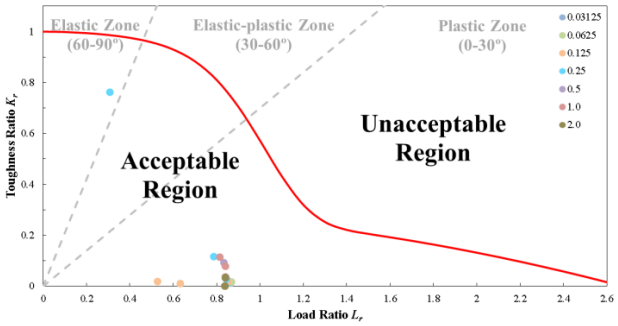

(b) P_N = 2, t/R_i = 0.1

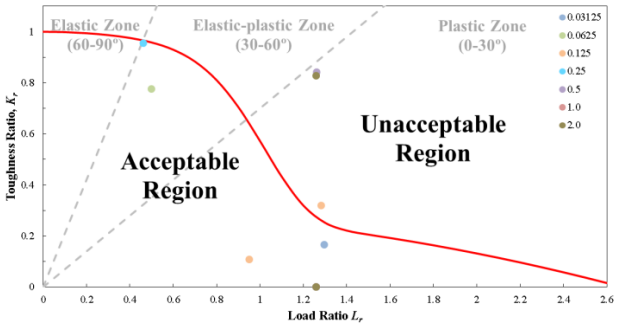

(c) P_N = 3, t/R_i = 0.1

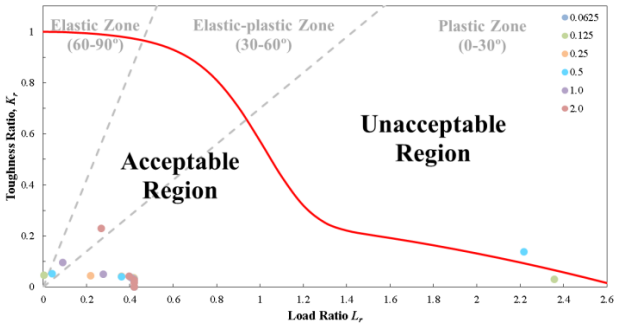

(d) P_N = 1, t/R_i = 0.2

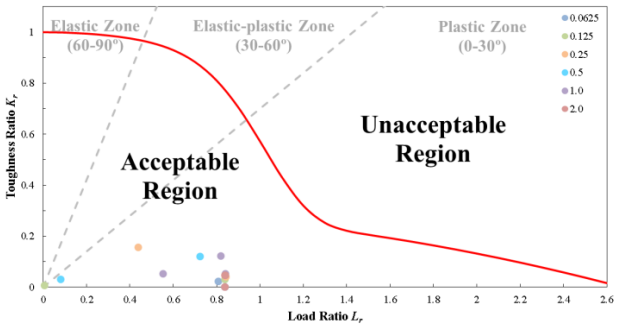

(e) P_N = 2, t/R_i = 0.2

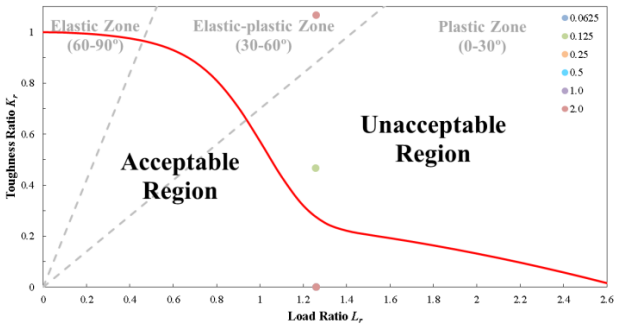

(f) P_N = 3, t/R_i = 0.2

Figure 12. Assessment points for flaw sizes at different P_N and t/Ri, along with crack length a/c (a-b-c-d-e-f);

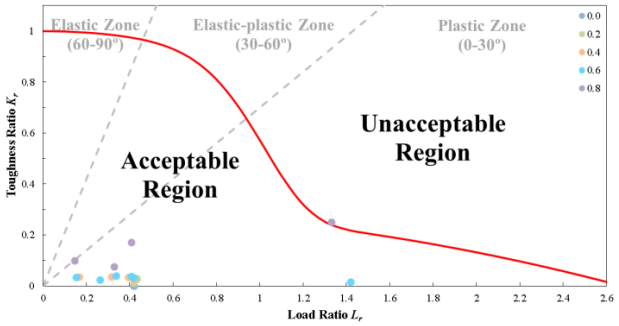

(g) $P_N = 1$, $t/R_i = 0.1$

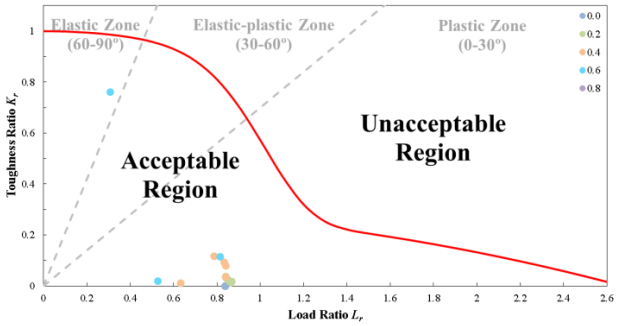

(h) $P_N = 2$, $t/R_i = 0.1$

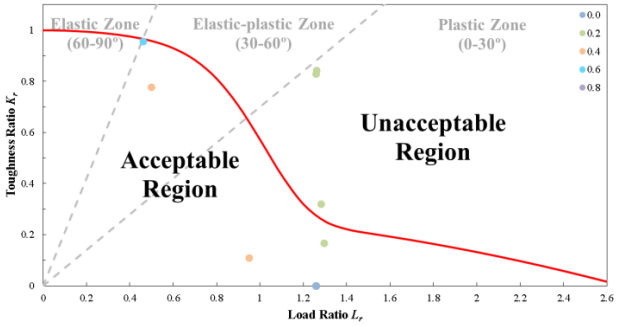

(i) $P_N = 3$, $t/R_i = 0.1$

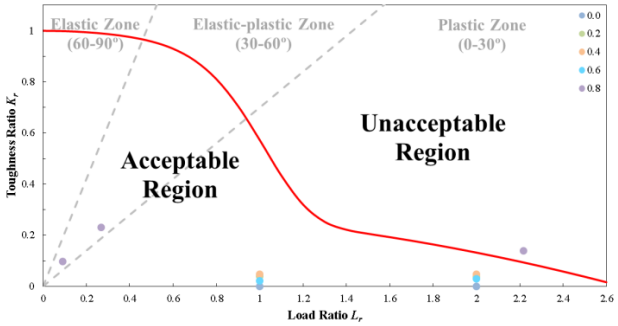

(j) $P_N = 1$, $t/R_i = 0.2$

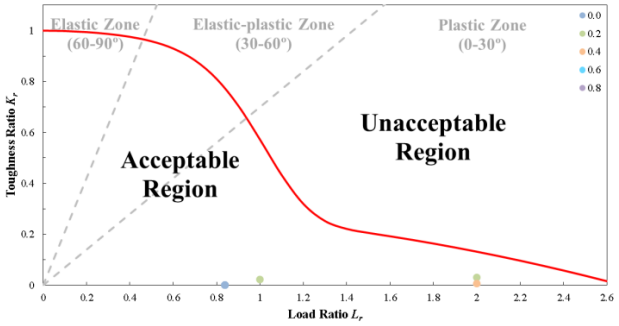

(j) $P_N = 2$, $t/R_i = 0.2$

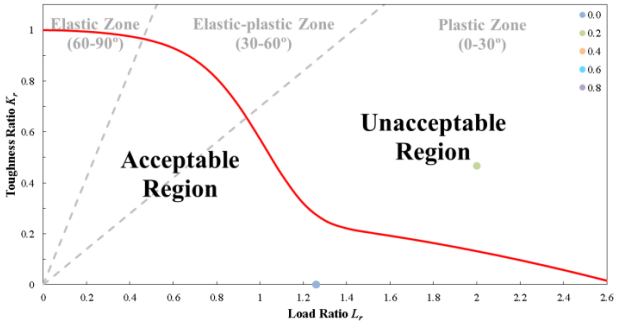

(j) $P_N = 3$, $t/R_i = 0.2$

Figure 12. (cont.) crack depth a/t (g-h-i-j-k-l)

3.5 Flaw Elliptical Angle (φ)

In Figure 13, assessment points are plotted against various normalized pressures P_N based on different flaw elliptical angles φ. This test of 15º, 30º, 45º, 60º, and 75º, respectively, reveals the elliptical angle at the time of the crack growth event. It is important to remember that the elliptical angle is the angle formed from the initial flaw size to the nth flaw size, as described in Figure 2(b). Generally, the distribution of assessment points predominantly leads to the plastic zone, even though the elliptical angle is small. From the initial clues, this can be attributed to the loading along with the material type of the spool pipe.

Compared to the flaw size explanation, the elliptical angle flaw shows a fully uniform effect at each assessment point. It is therefore sufficient to review the factors involved in the elliptical angle formation. Based on the results obtained, the load ratio L_r plays a greater role in failure assessment than the toughness ratio K_r. It is evident that the occurrence of assessment points, based on the variation of normalized pressure, increases at all elliptical angles. Moreover, this significant increase only occurs when $t/R_i = 0.2$. It can be observed that the thinner the thickness of the spool pipe, the greater the role of the elliptical angle on the flaw parameter, resulting in a large, unacceptable plastic collapse. On the other hand, the condition $t/R_i = 0.1$ is also influential, but only the consideration of increased loading makes a fundamental difference.

Furthermore, the results of several flawed elliptical angles show a very insignificant effect in determining the assessment point. This phenomenon can be understood by examining the shape function F, which exhibits a small profile when the crack intensity distribution, as defined by Eq. (24), is considered. The larger the elliptical angle, the effect of the toughness ratio K_r relatively does not contribute significantly. Therefore, the elliptical angle of the spool pipe is a simplifying factor in the case of flaw parameter determination when data is insufficient. Moreover, special consideration is needed in advance to accurately configure not only the crack length but also the crack depth.

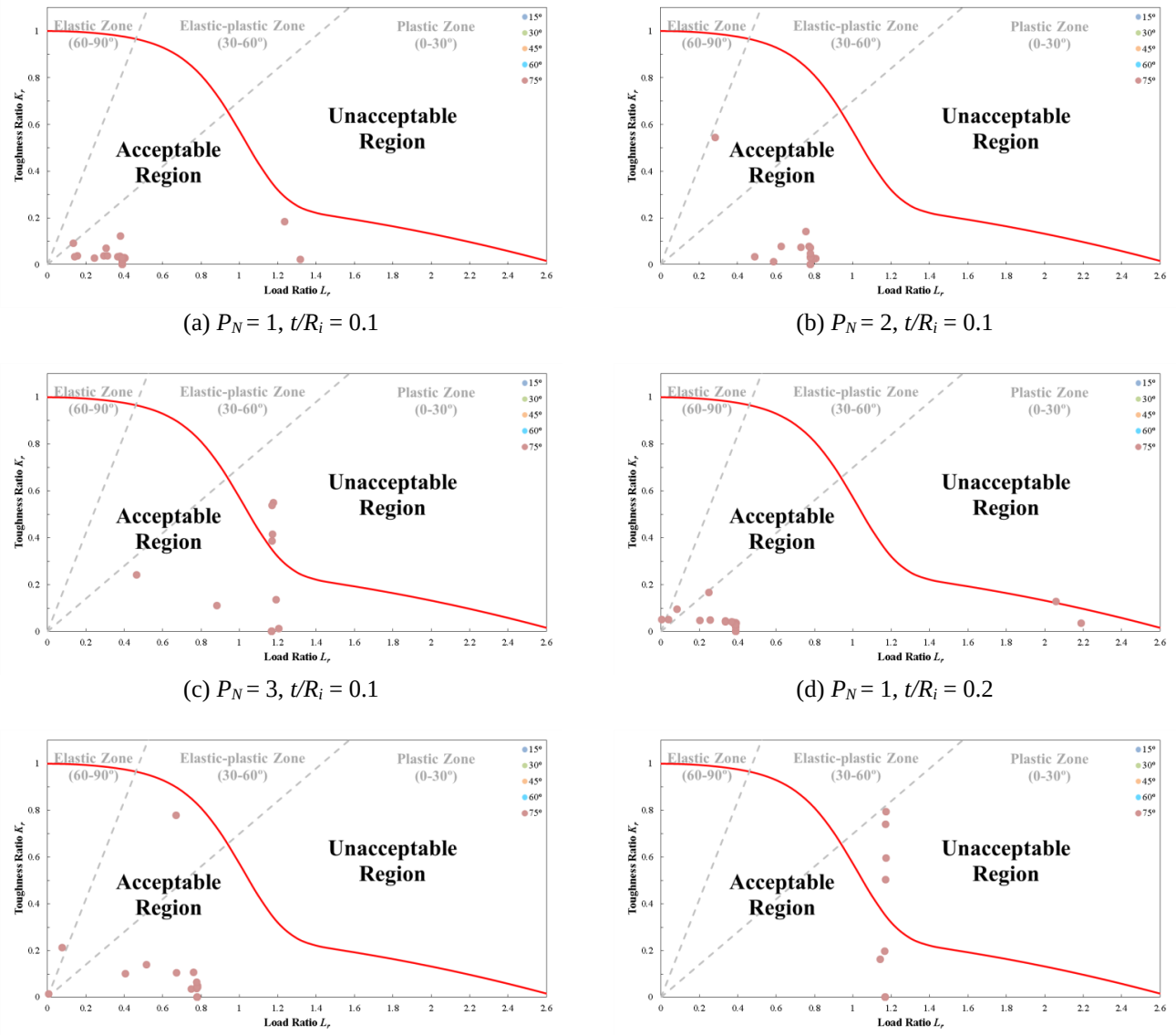

(a) $P_N = 1$, $t/R_i = 0.1$ (b) $P_N = 2$, $t/R_i = 0.1$

(c) $P_N = 3$, $t/R_i = 0.1$ (d) $P_N = 1$, $t/R_i = 0.2$

(e) $P_N = 2$, $t/R_i = 0.2$ (f) $P_N = 3$, $t/R_i = 0.2$

Figure 13. Assessment points for flaw elliptical angles φ at different P_N and t/Ri

4. CONCLUSIONS

The spool pipe was selected as the primary model for exploring the concept behind hydrotesting to observe crack propagation experimentally. The API 5L X65 spool pipe is designed to transport gas liquids. The accuracy level is adequate for hydrotesting. The test required two hours to complete, including the pressurizing and depressurizing operations. In experimental actuality, the pipe did not leak since the percentage of trapped air was approximately 0.006%. There was good agreement between the experimental data and the analytical trapped air approach. The pipeline's integrity was subsequently assessed to verify its compliance with the failure assessment diagram (FAD). The model surface has a semi-elliptical crack that moves circumferentially. The crack was likewise thought to be in the opening mode. Normalized pressure, material grades, flaw size, and flaw elliptical angle were all performed to assess the FAD's sensitivity. The sensitivities are summarized as follows:

i) Normalized pressures P_N ranging from 0.6 to 1.0 obtained feasible assessment points in each of the $t/R_i = 0.1$ and 0.2 situations using the declared data. It's also in the permitted plastic zone. When the P_N index exceeds 1.0, the stress intensity element becomes the primary cause of failure. According to this logic, the P_N index should be less than or equal to 1.

ii) Common material grades have a significant impact on failure assessment. This corresponds to the control of the toughness ratio K_r. Furthermore, the relationship between the t/R_i ratio and material grade has an impact on defining the assessment point. The greater the t/R_i ratio, the more probable the spool pipe material will fail. Therefore, selecting a grade equal to or higher than X65 is advised.

iii) The t/R_i ratio makes a significant contribution to determining crack length a/c and crack depth a/t, where the thin thickness of the spool pipe could accelerate the emergence of cracks. Furthermore, there is minimal impact on the correlation between a/c and load ratio L_r, and toughness ratio K_r. The transverse crack propagation mode is

diametrically opposed to the opening mode. The K_r ratio, on the other hand, has a substantial influence on *a/c*. This demonstrates the relevant influence in the crack growth inquiry. More specifically, it is estimated that *a/c* will be approximately 0.125 and *a/t* will be around 0.2.

iv) The typical impact is observed in the elliptic angle parameter φ. The L_r ratio, particularly t/R_i = 0.2, plays a larger role in identifying the failure point based on normalized pressure than the K_r ratio. Additionally, the most convincing evidence suggests that the influence of the crack shape function *F* is responsible for the relatively low-stress intensity factor observed in some of the reviewed elliptical angles. Therefore, if the completeness of the crack profile is not sufficient, the elliptical angle flaw can be simplified.

Despite the majority of plastic zones, the existing spool pipe is still considered appropriate. It can be reasonably deduced that the significant deformation that has occurred can be attributed to the absence of initial cracks. On the other hand, the most sensitive parameter among the others is flaw size. Not to mention that the toughness ratio K_r has a greater impact on crack propagation. Comparing the results of FAD to other methods, such as the remaining strength factor (RSF) is important for indicating the anticipated type of failure. Finite element (FE) modeling will also be implemented to validate further specifics of crack position against support interaction during hydrotesting [51]. Last but not least, recommendations for API 579 [24] address the limitation of t/R_i = 0.14 to guarantee the findings are not prematurely cautious.

ACKNOWLEDGEMENT

The authors express their gratitude to Laboratory Based Education (LBE) at the Faculty of Engineering, Universitas Hasanuddin: 11367/UN4.7.2/PM.01.01/2023 for their financial support on this study. The authors wish to acknowledge gratefully the contributions made by Mr. Slamet Wahyudi and his team (PT. Kaliraya Sari, East Kalimantan, Indonesia) by allowing us to conduct the mechanical testing for our research. Last but not least, the authors are grateful to anonymous reviewers for their constructive comments.

REFERENCES

[1] American Society of Mechanical Engineers (ASME), *Managing System Integrity of Gas pipelines*, 5th Edition. USA: ASME B31.8S, 2004.

[2] T. L. Anderson and G. V. Thorwald, "A finite element procedure to model the effect of hydrostatic testing on subsequent fatigue crack growth," in *Volume 1: Pipelines and Facilities Integrity*, American Society of Mechanical Engineers, 2016.

[3] B. Guo, S. Song, J. Chacko, and A. Ghalambor, *Offshore Pipelines*. Gulf Professional Publishing, 2005.

[4] American Society of Mechanical Engineers, *Gas Transmission and Distribution Piping Systems*. ASME B31.8-2007, 2007.

[5] American Society of Mechanical Engineers, *Pipeline Transportation Systems for Liquid Hydrocarbons and Other Liquids*. ASME B31.4-2006, 2006.

[6] International Standard Organization, *Petroleum and Natural Gas Industries-Pipeline Transportation Systems*. ISO 13623: 2000, 2000.

[7] National Association of Corrosion Engineers (NACE), *Inline Nondestructive Inspection of Pipelines*. Toronto, Canada: NACE International, Paper No. 35100, 2000.

[8] J. F. Keifner, *Hydrostatic Testing, GRI Guide for Locating and Using Pipeline Industry Research, Kiefner and Associates Incorporation for Gas Research Institute*. GR100.0192, 2001.

[9] P. Carr and I. F. J. Nash, "Eliminating the Precommissioning Hydrotest for Deepwater Gas Pipelines," in *International Offshore and Polar Engineering Conference*, Busan, Korea, 2014.

[10] J. F. Kiefner and W. A. Maxey, "The Benefits and Limitations of Hydrostatic Testing," in *API' s 51st Annual Pipeline Conference & Cybernetics Symposium*, New Orleans, LA, 2000.

[11] T. L. Anderson, G. Thorwald, D. J. Revelle, D. A. Osage, J. L. Janelle, and M. E. Fuhry, "Development of stress intensity factor solutions for surface and embedded cracks in API 579," *Welding Research Council Bulletin*, 2002.

[12] J. Cai, X. Jiang, and G. Lodewijks, "Residual ultimate strength of offshore metallic pipelines with structural damage – a literature review," *Ships and Offshore Structures*, vol. 12, no. 8, pp. 1037–1055, 2017.

[13] M. Staat, "Plastic collapse analysis of longitudinally flawed pipes and vessels," *Nuclear Engineering and Design*, vol. 234, no. 1–3, pp. 25–43, 2004.

[14] H. Ghaednia, S. Das, R. Wang, and R. Kania, "Dependence of burst strength on crack length of a pipe with a dent-crack defect," *Journal of Pipeline Systems Engineering and Practice*, vol. 8, no. 2, 2017.

[15] H. Ghaednia, S. Das, R. Wang, and R. Kania, "Effect of operating pressure and dent depth on burst strength of NPS30 linepipe with dent–crack defect," *Journal of Offshore Mechanics and Arctic Engineering*, vol. 137, no. 3, 2015.

[16] H. Ghaednia, S. Das, R. Wang, and R. Kania, "Safe burst strength of a pipeline with dent–crack defect: Effect of crack depth and operating pressure," *Eng Fail Anal*, vol. 55, pp. 288–299, 2015.

[17] B. Bedairi, D. Cronin, A. Hosseini, and A. Plumtree, "Failure prediction for Crack-in-Corrosion defects in natural gas transmission pipelines," *International Journal of Pressure Vessels and Piping*, vol. 96–97, pp. 90–99, 2012.

[18] A. Okodi, Y. Li, R. Cheng, M. Kainat, N. Yoosef-Ghodsi, and S. Adeeb, "Crack propagation and burst pressure of pipeline with restrained and unrestrained concentric dent-crack defects using extended finite element method," *Applied Sciences*, vol. 10, no. 21, p. 7554, 2020.

[19] A. Okodi, M. Lin, N. Yoosef-Ghodsi, M. Kainat, S. Hassanien, and S. Adeeb, "Crack propagation and burst pressure of longitudinally cracked pipelines using extended finite element method," *International Journal of Pressure Vessels and Piping*, vol. 184, p. 104115, 2020.

[20] X. Liu, "Numerical and experimental study on critical crack tip opening displacement of X80 pipeline steel," *Mechanics*, vol. 23, no. 2, pp. 204 - 208. 2017.

[21] T. L. Anderson, *Stress Intensity and Crack Growth Opening Area Solutions for Through-wall Cracks In Cylinders And Spheres*. WRC Bulletin 478, Welding Research Council, 2003.

[22] National Energy Board, "National Energy Board Report of the Inquiry on Stress Corrosion Cracking on Canadian Oil and Gas Pipelines," 1996.

[23] British Standard Institute, *Guide on Methods for Assessing the Acceptability of Flaws in Metallic Structure BS 7910*. British Standard Institute, 1999.

[24] *API RP 579-1 / ASME FFS-1, API 579-1/ASME FFS-1*, Third Edition. New York, USA: The American Society of Mechanical Engineers, 2016.

[25] S. Cicero, S. Arrieta, M. Sánchez, and L. Castanon-Jano, "Analysis of additively manufactured notched PLA plates using failure assessment diagrams," *Theoretical and Applied Fracture Mechanics*, vol. 125, p. 103926, 2023.

[26] S. Cicero, M. Sánchez, V. Martínez-Mata, S. Arrieta, and B. Arroyo, "Structural integrity assessment of additively manufactured ABS, PLA and graphene reinforced PLA notched specimens combining Failure Assessment Diagrams and the Theory of Critical Distances," *Theoretical and Applied Fracture Mechanics*, vol. 121, p. 103535, 2022.

[27] S. Cicero, V. Madrazo, I. A. Carrascal, and R. Cicero, "Assessment of notched structural components using Failure Assessment Diagrams and the Theory of Critical Distances," *Engineering Fracture Mechanics*, vol. 78, no. 16, pp. 2809–2825, 2011.

[28] D. Wang, A. B. Hagen, P. U. Fathi, M. Lin, R. Johnsen, and X. Lu, "Investigation of hydrogen embrittlement behavior in X65 pipeline steel under different hydrogen charging conditions," *Materials Science and Engineering: A on ScienceDirect*, vol. 860, p. 144262, 2022.

[29] E. Ohaeri, U. Eduok, and J. Szpunar, "Hydrogen related degradation in pipeline steel: A review," *International Journal of Hydrogen Energy*, vol. 43, no. 31, pp. 14584–14617, 2018.

[30] L. Ligang *et al.*, "Evaluation of the fracture toughness of X70 pipeline steel with ferrite-bainite microstructure," *Materials Science and Engineering: A*, vol. 688, pp. 388–395, 2017.

[31] A. Coseru, J. Capelle, and G. Pluvinage, "On the use of Charpy transition temperature as reference temperature for the choice of a pipe steel," *Engineering Failure Analysis*, vol. 37, pp. 110–119, 2014.

[32] X. Gao, Y. Shao, L. Xie, Y. Wang, and D. Yang, "Prediction of Corrosive Fatigue Life of Submarine Pipelines of API 5L X56 Steel Materials," *Materials*, vol. 12, no. 7, p. 1031, 2019.

[33] S. Capula-Colindres, G. Terán, D. Angeles-Herrera, J. C. Velázquez, and E. Torres-Santillán, "Determination of Fracture Toughness and KIC-CVN Correlations for BM, HAZ, and WB in API 5L X60 Pipeline," *Arabian Journal for Science and Engineering*, vol. 46, no. 8, pp. 7461–7469, 2021.

[34] M. Soudani *et al.*, "Reduction of hydrogen embrittlement of API 5l X65 steel pipe using a green inhibitor," *International Journal of Hydrogen Energy*, vol. 43, no. 24, pp. 11150–11159, 2018.

[35] D. Wang, A. B. Hagen, D. Wan, X. Lu, and R. Johnsen, "Probing hydrogen effect on nanomechanical properties of X65 pipeline steel using in-situ electrochemical nanoindentation," *Materials Science and Engineering: A on ScienceDirect*, vol. 824, p. 141819, 2021.

[36] E.E. Cota, "Toughness Evaluation and Fracture Predictions in Elastoplastic Materials," Ph.D Thesis, Pontifícia Universidade Católica do Rio de Janeiro, Brazil, 2019.

[37] Design Engineering Practice (DEP), *Hydrostatic Pressure Testing of New Pipelines, Design and Engineering Practice, Technical Specification for Royal Dutch/ Shell Group*. DEP 31/40/38/Gen, 1993.

[38] E.W. McAllister. Pipeline Rules of Thumb Handbook, 5th ed. Elsevier BV, 2009.

[39] J. C. Gray, "How Temperature Affects Pipeline Hydrostatic Testing," *Pipeline and Gas Journal*, vol. 203, no. 14, p. 30, 1976.

[40] T. Lewis and X. Wang, "The T-stress solutions for through-wall circumferential cracks in cylinders subjected to general loading conditions," *Engineering Fracture Mechanics*, vol. 75, no. 10, pp. 3206–3225, 2008.

[41] Y. H. Wang, G. Z. Wang, S. T. Tu, and F. Z. Xuan, "In-plane and out-of-plane constraint characterization of different constraint parameters for semi-elliptical surface cracks in pipes*," Engineering Fracture Mechanics*, vol. 235, p. 107161, 2020.

[42] C. E. Feddersen, "Evaluation and Prediction of the Residual Strength of Centre Cracked Tension Panels," American Standard Testing and Material, STP26673S, p. 50, 1970.

[43] M. Palmer, *Pressure Testing Procedures for Pipelines, Facilities Engineering, Maintenance and Construction (FEMC)*, Revision 2. Revision 2, No- EN/MPS/706, 2004.

[44] American Institute of Petroleum (API), *Recommended Practice for the Pressure Testing of Steel Pipelines for the Transportation of Gas, Petroleum Gas, Hazardous Liquids, Highly Volatile Liquids or Carbon Dioxide*, Sixth Edition. USA: Institute of Petroleum, 2013.

[45] Californa State Land Commission (CSLC), *A Procedure for the Hydrostatic Pressure Testing of Marine Facility Piping*. USA: California State Lands Commission, 2003.

[46] R. Verley, S. Lund, and H. Moshagen, "Wall thickness design for high pressure offshore gas pipelines," in *American Society of Mechanical Engineers*, New York, USA, 1994.

[47] T. Sotberg and R. Burschi, "Future pipeline design philosophy-framework" in *The International Conference on Offshore Mechanics and Arctic Engineering*, American Society of Mechanical Engineers, pp. 239–239, 1992.

[48] American Institute of Petroleum (API), *Specification for Line Pipe*, 43th Edition. USA: Institute of Petroleum, 2004.

[49] Q. Bai and Y. Bai, "Wall Thickness and Material Grade Selection," in *Subsea Pipeline Design, Analysis, and Installation*, Elsevier, pp. 23–39, 2014.

[50] G. Jiao, T. Sotberg, R. Bruschi, R. Verley, and K. Moerk, "The SUPERB project: Wall thickness design guideline for pressure containment of offshore pipelines (No. CONF-9606279-)," New York, United State: American Society of Mechanical Engineers, 1996.

[51] A. Bahadori, "Transportation Pipelines Pressure Testing," in *Oil and Gas Pipelines and Piping Systems*, Elsevier, pp. 93–117, 2017.